Supraglacial streams drive widespread partial-depth hydrofractures in ice sheets

David Chandler[1*] and Alun Hubbard[2,3]

[1*]NORCE Norwegian Research Centre and Bjerknes Centre for Climate Research, Bergen, Norway.
[2]Centre for Arctic Gas Hydrate, Environment and Climate, Department of Geosciences, UiT The Arctic University of Norway, Tromsø, Norway.
[3]Geography Research Unit, University of Oulu, Oulu, Finland.

*Corresponding author(s). E-mail(s): dcha@norceresearch.no; Contributing authors: ahu012@uit.no;

Abstract

Dramatic supraglacial lake drainage events in Greenland and Antarctica are enabled by rapid hydrofracture propagation through >1 km ice. Here, we present a slower mode of hydrofracture, where hairline surface fractures intersect supraglacial streams, and hypothesise that penetration depth is critically limited by water supply and englacial refreezing. We apply a novel model of stream-fed hydrofracture to the Greenland Ice Sheet and find that under most conditions, 2-cm-wide fractures can penetrate hundreds of metres before freezing closed. Conditions for full-depth hydrofracture are more restricted, requiring larger meltwater channels and/or warm englacial conditions. Given the abundance of streams and surface fractures across Greenland and Antarctica's expanding ablation zones, we propose that stream-driven hydrofractures are ubiquitous – even where distant from supraglacial lakes and crevasse fields. This intriguing process remains undetectable by current satellite remote-sensing, yet has two major thermodynamic impacts that warrant further investigation. First, by driving widespread cryohydrologic warming at depths far greater than surface crevassing, it explains a consistent cold bias in modelled englacial thermal profiles. Second, the associated reduction in ice viscosity and increased damage accumulation act to enhance the vulnerability of ice sheets and shelves to dynamic instability as supraglacial drainage networks expand to reach higher elevations.

Keywords: Ice sheet, hydrofracture, hydrology, dynamics

Abrupt supraglacial lake drainage events, driven by hydrofracture, have been reported from the Greenland Ice Sheet [1–3] and Antarctic ice shelves [4, 5]. In Greenland, rapid hydrofracture has been observed to drain $>10^7$ m^3 of melt water through >1 km of ice in a matter of hours, driving meter-scale hydraulic uplift with distinct seismic, tectonic and dynamic signatures [1–3, 6]. However, the long-term dynamic impacts of lake drainage events remain ambiguous [7–9]. In Antarctica, lake-driven hydrofracturing is currently observed only on floating ice shelves, where it has been observed to trigger ice shelf disintegration [5, 10] and, by reducing buttressing, can lead to the destabilisiation of upstream ice [11].

Here we consider a less dramatic mode of hydrofracture where thin surface fractures intersect supraglacial stream networks. During fieldwork in the ablation zone of the Greenland Ice Sheet [12, 13], we have observed the opening of abundant hairline fractures associated with ice flow acceleration following the onset of seasonal melt (Figs. ED1-ED3). Typically, we observed sets of multiple parallel thin fractures extending hundreds of metres perpendicular to prevailing ice flow, even across zones distant from crevasse fields and supraglacial lakes. The fractures were generally 1 to 2 cm wide [13] and hence remain undetectable in satellite or UAV remote-sensing observations [14]. Due to their apparent ubiquity, we propose that such surface fractures – if they can initiate hydrofractures – will have two important impacts on ice dynamics even if they do not all attain the bed and develop into moulins. First, the latent heat release when meltwater refreezes at depth causes englacial warming (known as cryohydrologic warming), and associated viscous softening [15–18]; and second, the fracturing itself contributes to increasing englacial damage accumulation that promotes downstream calving [19, 20].

As not all surface fractures that intersect supraglacial streams develop into moulins, we hypothesise that the critical constraint for stream-driven hydrofracturing is the balance between water supply and englacial refreezing. Water supply is limited by a combination of factors: (i) the short length of fracture, typically less than a few meters, underlying the stream; (ii) supraglacial channels are often choked with snow in early summer, which impedes water flow; and (iii) the hydraulic head (stream depth) driving water into an underlying fracture is typically <2 m, whereas supraglacial lakes commonly attain depths >5 m [21–23]. Previous theoretical work suggests that surface fractures attain the bed of an ice sheet provided there is sufficient water available to maintain a full fracture [24–28]. Here we consider the dimensions of observed hairline surface fractures and supraglacial streams, and develop a model of hydrofracture propagation in cold ice where meltwater supply is limited. We apply the model to six locations on the Greenland Ice Sheet where down-borehole temperature and ice thickness measurements are available (Fig. 1).

The sites are geographically constrained by the availability of boreholes instrumented with thermistor strings, but represent a wide range of ice thickness and flow conditions in west Greenland's land- and marine-terminating glaciers.

Stream-driven hydrofracture

Our model calculates the downwards propagation rate of a surface fracture of length L_f and width w_f in ice of thickness H (Fig. 2 and Methods). With z as the vertical co-ordinate (increasing downwards from zero at the ice surface), the fracture tip is at z_d and the water level is at $z_a < z_d$. We assume the fracture intersects a supraglacial stream with semi-circular cross section (radius r_c). The model calculates fracture propagation depth using van der Veen's [25] linear elastic fracture mechanics, and the water filling rate due to leakage from the channel is based on Toricelli's equation [29]. It is this leakage rate that limits fracture propagation rate. Starting with a shallow air-filled fracture, at each time step the model calculates the change in water level in the fracture, and then the new propagation depth. Refreezing by ice accretion onto the fracture walls at each level in the fracture is finally calculated following Alley et al. [26], but here we apply observed temperature profiles and the duration for which that level has been submerged. Fractures in which the accreted ice reaches the full fracture width are likely to become blocked, preventing further propagation. Therefore, blockage is more likely for thinner fractures, smaller supraglacial channels (slower leakage rate), or colder englacial ice.

We also consider two end-member cases of feedback between water flow and fracture aperture enlargement beneath the channel by viscous heat dissipation. In the first case we neglect any aperture enlargement, and thus implicitly underestimate meltwater supply and fracture propagation rate (the 'slow model'). In the second we use a simple treatment of this complex process, which likely overestimates aperture enlargement and fracture propagation rate (the 'fast model'). Hence, a reasonable estimate for propagation rate should lie between these two end-member limits.

Results

To indicate the conditions under which thin ($\sim$2 cm) hydrofractures may become occluded by refreezing before reaching the bed, in Figs. 3 and 4 we use stippling to indicate possible occlusion (1 to 3 cm ice accretion) and hatching to indicate likely ice occlusion (>3 cm ice accretion).

Our 'slow' model with limited water supply demonstrates that thin fractures intersecting a supraglacial stream only propagate sufficiently fast to attain the bed under very restricted conditions in west Greenland. These conditions are site-specific, but typically require relatively short fractures or large channels (Fig. 4). A notable exception is the relatively thin, warm ice near the margin (Bowdoin Glacier BH2; Paaqitsoq GULL). Otherwise, fractures become occluded by accreting ice and are sealed shut before reaching the bed. Both ice thickness and temperature are critical constraints on propagation

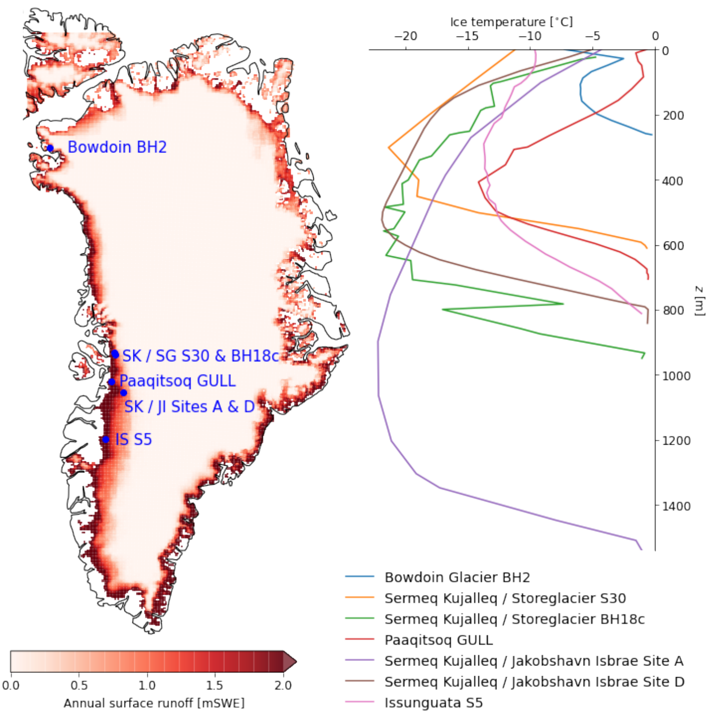

Fig. 1 Left: locations of measured temperature profiles, including those used in Figs. 3 and 4. The sites are: BH2 on Bowdoin Glacier [18], sites S30 and BH18c on Sermeq Kujalleq / Storeglacier (SK / SG) [30, 31], GULL in the Paakitsoq region [17], Site A on Sermeq Kujalleq / Jakobshavn Isbrae (SK / JI) [32], and Site S5 on Issunguata Sermia (IS) [33]. Shading is mean annual runoff (melt and rainfall) for ice-covered regions during the period 2000 to 2019, as calculated by Collosio et al. [34] using the Modèle Atmosphérique Régional (MAR) v3.11.2 forced by ERA5 reanalysis [35]. Right: the respective temperature profiles at the borehole sites.

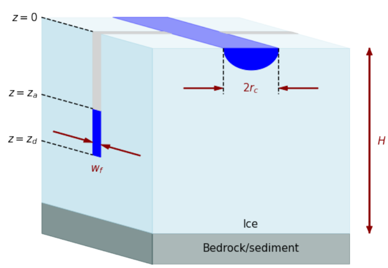

Fig. 2 Schematic showing key components of our model. Here a fracture of depth z_d, with water level z_a, is being filled by water from a supraglacial channel with radius R_c. The ice thickness is H.

depth, as demonstrated by comparison of results in Figs. 3 and 4 for SK/Store S30 and Paaqitsoq GULL (similar thickness, but SK/Store S30 is colder), or for SK/Store S30 and SK/JI Site A (similar minimum temperatures but Site A is much thicker). Fracture width is also an important constraint, with 1 cm wide fractures being far more prone to occlusion than 3 cm wide fractures: this is evident by the extensive stippled areas but more restricted hatched areas in Figs. 3 and 4.

With our 'fast' model that likely overestimates water supply, 1 cm wide fractures remain liable to occlusion (except at Bowdoin). However, because there is less ice accretion than with the 'slow' model, full-depth propagation of wider (2 to 3 cm) hydrofractures is noticeably less restricted, becoming possible under most conditions. Exceptions are fractures fed by small ($r_c < 0.5$ m) channels at SK/Store S30 and SK/JI Site A, where the ice column is relatively cold due to rapid advection of inland ice, and is over 1000 m thick.

Assuming that hydrofracture propagation continues unimpeded until ice accretion reaches the full fracture width (indicated by the stippling and hatching in Fig. 3), even relatively narrow surface fractures will propagate several hundred metres before becoming choked by ice. Narrow fractures hence contribute to considerable englacial latent heat release (cryohydrological warming: methods, and Fig. 5) and damage accumulation even at locations where they cannot initiate moulin development. Indeed it is this scenario that is most intriguing, as the process is likely ubiquitous across Greenland's densely fractured ablation zone, affecting much deeper ice than would otherwise be reached by surface crevasses, yet remaining undetected by satellite remote sensing.

With limited water supply, propagation times may be well in excess of 12 hours. During this time the channel water level is likely to have decreased from its assumed initially full level, owing to surface melt-driven diurnal changes in supraglacial stream discharge [13, 36]. Accounting for this diurnal variability by assuming sinusoidal changes in leakage over diurnal time scales (see Methods), delays propagation and generally allows more ice accretion (Figs. ED5-ED6). Interestingly, in contrast to Fig. 4 the maximum ice accretion does not necessarily increase monotonically with decreasing r_c and increasing L_f. This is related to the time the fracture reaches the coldest ice, relative to the times when leakage and propagation are slower. Overall the importance of diurnal variability increases for longer propagation times (e.g., in the 'slow' model with thicker ice or smaller channels), and will likely depend on the extent to which the diurnal streamflow variability is delayed and attenuated by site-specific characteristics of the upstream supraglacial catchment [13, 36].

Limitations

Our model pragmatically assumes an idealised planar fracture geometry, though at present there is little field evidence to indicate what this geometry should be, or how it might be affected by site-specific conditions such as basal topography. Partial support may come from structural glaciological

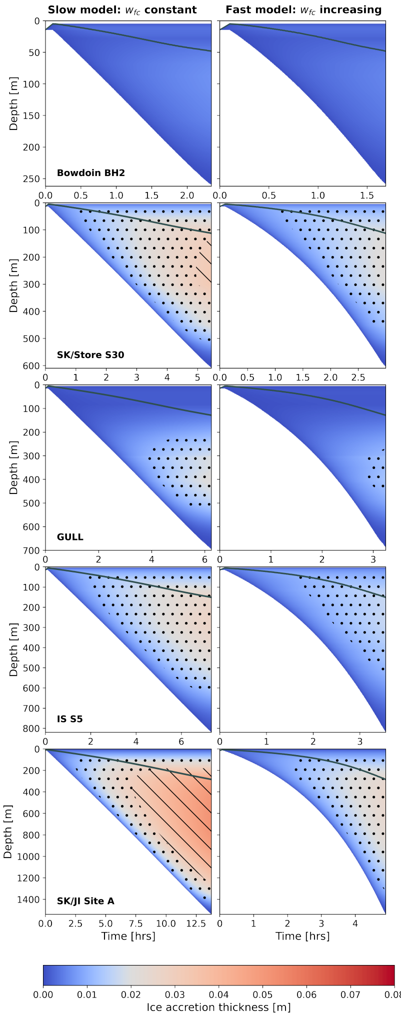

Fig. 3 Temporal evolution of fracture propagation and ice accretion. Fracture propagation is modelled following van der Veen [25] (see Methods). The lower edge of the shading shows the fracture depth, and the water level is shown by the solid grey line. Shading indicates the thickness of ice accretion on to the fracture walls (Eq. 9), with stippling and hatching indicating where total ice accretion is sufficient to close fractures of width 1 or 3 cm, respectively. These examples used $L_f = 250$ m, $r_c = 1.0$ m based on observations in SW Greenland [13], and the measured borehole temperature profiles shown in Fig. 1. Note that propagation rate is independent of fracture width w_f (see Methods).

observations of similar regular fractures where exposed at the margins of a polythermal glacier in Svalbard [37] and at Isungata Sermia (labeled IS S5 in Fig. 1), a land-terminating outlet of the Greenland ice sheet [14]. Theoretical fracture width profiles [24, 38] are not consistent with our observations, as the upper part of the fracture becomes pinched closed when water supply is limited

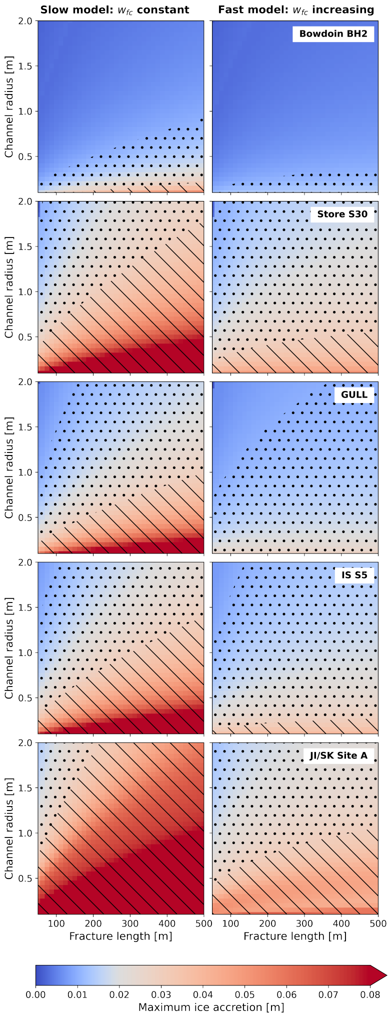

Fig. 4 Maximum ice accretion thickness in fractures propagating to the bed. Maximum ice accretion is an indication of the minimum fracture width needed to enable full-depth hydrofracture propagation; thinner fractures will terminate before reaching the bed. Shading indicates the ice accretion thickness (Eq. 9), with stippling and hatching indicating where total ice accretion is sufficient to close fractures of width of 1 or 3 cm, respectively. These examples used the measured borehole temperature profiles shown in Fig. 1.

(see Methods). The simultaneous upward propagation of basal hydrofractures [39, 40] could act to decrease the timescale required to establish a full-depth fracture that connects with the subglacial drainage system, making moulin development more likely since there is less time for ice to accrete in the fracture. Clearly, accounting for the geometry of surface and/or basal crevasses, and estimating if/where they are likely to intersect, would be a useful development but requires significantly more observational constraints than currently available, along with more sophisticated modelling at specific sites.

In the mid to upper ablation zone where the water supply limit becomes critical due to the colder, thicker ice, large meltwater streams are relatively sparsely distributed. However, a fracture extending laterally for some hundreds of metres will inevitably intersect other smaller channels, as well as the main channel. Indeed, multiple small moulins are frequently observed along fracture lines even in ice over 1000 m thick, and presumably connect laterally at depth in the fracture. These smaller water sources do not substantially alter the outcome of our results, since: (1) the water supply q from each channel depends on $r_c^{3/2}$, so smaller streams contribute disproportionately less water; and (2) at the time when the fractures are observed to open [13], many small channels are still choked with slush, and are limited in their capacity to supply water. Surface surveys of fracture zones and early-season supraglacial stream networks would enable better estimates of the contributions from smaller channels.

Multiple cycles of hydrofracturing can potentially overcome the limitation of refreezing, and successively enable fractures to propagate more deeply. For example, if the fracture freezes closed before connecting with the bed, then released latent heat will have warmed the surrounding ice, allowing it to propagate further in a subsequent cycle. However, accommodating the accumulation of new ice at depth in each cycle would cause progressive widening of the surface fractures, in contrast to our observation that surface fractures remain less than $\sim$2 cm in width rather than undergoing successive expansion [13]. Another hindrance to multiple cycles is the decreasing water level as the fracture propagates (Fig. 3). By the time the fracture freezes closed, the water level may have dropped almost to the point where the fracture is occluded by ice. Reopening that part of the fracture requires additional filling, allowing further refreezing below the blockage. Finally, the transient tensile stress state that induced the initial fracturing may gradually be released by viscous creep, or could even transition into compressive stress if there is moulin development and ice acceleration up-glacier [41]. Both of these scenarios act to limit the efficacy of subsequent cycles of hydrofracture.

Alternative fracture propagation models [27, 28, 38, 42] are qualitatively consistent with van der Veen [25]: specifically, dry fractures cannot penetrate to the bed, while water-filled fractures can (with the exception of shallow, narrow water-filled fractures considered by Alley et al. [26], which cannot reach the bed). Providing that a water level *near* to the surface is required to propagate the fracture, then the process enabling that propagation is unlikely to greatly affect our results presented here, since we find that the rate and depth of propagation is still critically limited by water supply. Hence, unless the fracture process itself influences the geometry of the fracture, it is likely that uncertainties in the water filling rate rather than the choice of propagation model will act as the main source of uncertainty in our results. Nevertheless, further work to explore how irregularities in fracture geometry and ice accretion could lead to positive feedback that generates preferential flow paths (similar to subglacial channel development from sheet flow [43]), would help to better quantify the effects of these fractures.

Implications for ice sheets

Our observations and model demonstrate the clear potential for widespread partial-depth hydrofractures, and also limited moulin development from full-depth hydrofractures, initiated by fractures that intersect supraglacial stream networks on ice sheets. This result is relevant across the extensive ablation zone of the Greenland Ice Sheet (Fig. 1), extending above the equilibrium line into the wet-firn zone where hydrological controls on ice flow remain uncertain [7–9]. In these upper regions, moulin initiation may be restricted to supraglacial lake drainage events, or to intercepts of streams much larger than those considered here (e.g., Fig. ED1). This is significant due to the contrasting dynamic responses of abrupt supraglacial lake drainage events and slow/gradual moulin development from stream intercepts, and because of the sparse distribution of lakes relative to the dense network of streams.

Partial-depth hydrofracturing readily explains the consistent cold bias apparent in modelled temperature profiles when compared with observations in Greenland [16, 17, 33, 40]. Although the efficacy of cryohydrologic warming as a mechanism for ice acceleration and dynamic thinning has been argued to be limited in Greenland under present conditions [44, 45], this likely reflects an underestimate of its magnitude. For example, our results indicate that stream-driven hydrofracture will enable deeper and more widespread latent heat release than that assumed by Poinar et al.[45], where heating was limited to the upper ∼300 m across regions with open crevasses. In our methods we demonstrate that resulting warming can reach 1K per 10 km along-flow even with conservative estimates for fracture density (Fig. 5). Significantly, deeper latent heat release will be disproportionately more effective at enhancing ice flow, due to the nonlinear thermal-dependence and rheology of ice. Furthermore, lower ice viscosity enables greater transverse strain rates, and stronger velocity gradients across shear margins, so that fast-flowing outlet glaciers and ice streams are less impeded by their margins. Therefore, as surface melting extends into the higher-elevation interior, this enhanced englacial warming potentially contributes to ice acceleration and dynamic instability in ice sheets.

Our analysis is increasingly relevant to the Antarctic Ice Sheet in a warming climate. Hydrofracture has been observed to trigger ice shelf collapse [4, 5, 46, 47], and although this is driven by surface ponding where water supply is not a limiting factor, climate warming will promote increasing melting and supraglacial stream development across ice shelves and upstream grounded ice [48, 49] in a situation increasingly analogous to Greenland at present. Indeed, supraglacial drainage systems are already observed on grounded ice in West Antarctica and the Peninsula [48, 50]. Whether stream-fed hydrofractures can stabilise ice shelves by reducing supraglacial lake volumes [51], or destabilise ice shelves via the latent heat and/or damage accumulation discussed above, remains an open question. Nevertheless, the prospect of deep cryohydrologic warming and reduced viscosity within Antarctica's ice streams should be sufficient motivation for further investigation into this emerging feedback process.

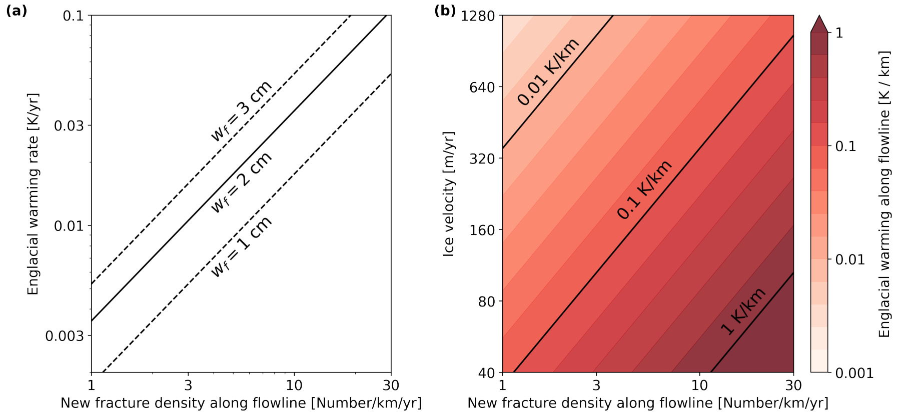

Fig. 5 Englacial warming due to latent heat released by stream-driven hydrofractures. (a) Warming rates dT_f/dt calculated using Eq. 19, which apply at depths reached by partial depth hydrofractures – perhaps several hundred metres (Fig. 3), much deeper than open crevasses. (b) The cumulative effect of seemingly small warming rates in Part (a) is apparent when converting the time derivative to a spatial derivative (Eq. 20), for representative conditions in land- and marine-terminating outlets in West Greenland. Warming scales linearly with fracture width w_f; this plot used $w_f = 2$ cm.

Summary

Despite its simplicity, our model provides strong evidence that supraglacial streams are capable of driving widespread, partial-depth hydrofractures through cold ice, under a wide range of conditions representative of those encountered on the Greenland Ice Sheet – and perhaps in Antarctica under future warming. Significantly, this process is likely to be ubiquitous even outside of regions with lakes or visible crevasses, as narrow (1 to 2 cm) fractures are abundant in the ice sheet ablation zone [13, 15]. Therefore, hydrofracturing beneath streams can cause strong englacial warming in relatively thick ice ($>$ 1 km) where full-depth hydrofractures and moulin development are dependent on lakes or unusually large channels. Noting that this mode of hydrofracturing will be very difficult to observe in remote sensing images, in contrast to widely-observed lake drainages [22, 52–54], we clearly need more ground-based observations of the interaction between supraglacial streams and thin fractures. With the aid of these observations, future modelling efforts will help to constrain the magnitude of deep englacial warming or damage accumulation, and its contribution to dynamic flow instability in Greenland and Antarctica under present and future conditions.

Methods

The downwards propagation of hydrofractures in ice sheets is similar in principle to the upwards propagation of dikes in the Earth's crust [24, 26, 55]. Hence, the model we develop below draws on previous work in both situations.

Van der Veen's theory

We consider a surface fracture reaching depth d in ice of thickness H, where the 'far field' resistive tensile stress is R_{xx} (Fig. 2). With z as the vertical coordinate (increasing downwards from zero at the surface), the fracture tip is at z_d and the water level is at $z_a < z_d$. The fracture will propagate downwards provided the elastic stress intensity factor K_I at the fracture tip exceeds a threshold K_{Ic}, known as the fracture toughness [25]. In glaciers, K_{Ic} is loosely estimated as 0.1 to 0.4 MPa$^{1/2}$ [25].

K_I is the sum of three components, corresponding to the tensile stress ($K_I^{(1)}$), ice overburden pressure ($K_I^{(2)}$), and water pressure ($K_I^{(3)}$). Following van der Veen [25] these are:

$$K_I^{(1)} = F(\lambda) R_{xx} \sqrt{\pi d} \tag{1}$$

$$K_I^{(2)} = \frac{-2\rho_i g}{\sqrt{\pi d}} \int_0^{z_d} z G(\gamma, \lambda) dz \tag{2}$$

$$K_I^{(3)} = \frac{2\rho_w g}{\sqrt{\pi d}} \int_{z_a}^{z_d} (z - z_a) G(\gamma, \lambda) dz \tag{3}$$

Here, R_{xx} is the resistive longitudinal stress [56], which is assumed constant with depth; $\lambda = d/H$; $\gamma = z/d$; and the empirical functions $F(\lambda)$ and $G(\gamma, \lambda)$ are [25, 57]:

$$F(\lambda) = 1.12 - 0.23\lambda + 10.55\lambda^2 - 21.72\lambda^3 + 30.39\lambda^4. \tag{4}$$

$$\begin{aligned} G(\gamma, \lambda) = & \frac{3.52(1-\gamma)}{(1-\lambda)^{3/2}} - \frac{4.35 - 5.28\gamma}{(1-\lambda)^{1/2}} \\ & + \left[\frac{1.30 - 0.30\gamma^{3/2}}{(1-\gamma^2)^{1/2}} + 0.83 - 1.76\gamma \right] \times [1 - (1-\gamma)\lambda] \end{aligned} \tag{5}$$

Eq. 2 is a simplified version of Eq. 14 in van der Veen [25], since in the ablation zone we assume ice density is constant with depth. For air-filled fractures ($K_I^{(3)}$=0), Eqs. 1 and 2 predict that the total stress intensity $K_I = K_I^{(1)} + K_I^{(2)}$ exceeds K_{Ic} only for fractures shallower than ∼20 m in a 'typical' case (R_{xx}= 100 kPa, H = 200 to 2000 m). Even under an 'extreme' high tensile stress of

R_{xx}= 1000 kPa, then $K_I > K_{Ic}$ only for fractures penetrating ~200 m into ice 1000 m thick. This explains why the model has predicted air-filled surface fractures cannot penetrate to the bottom of glaciers under most circumstances [58]. However, as the fracture fills with water, the higher density of water compared to ice allows a water-filled fracture to penetrate to the bed even in thick ice – except where prevented by refreezing [26] – consistent with predictions of other theoretical and numerical studies [26, 27, 42, 59].

Fracture propagation through cold ice with limited water supply

As a fracture propagates downwards and its volume increases, a continued supply of water is needed to maintain a high water level. van der Veen [58] used a simplified version of the above theory to provide a time scale for fracture growth under a limited (but arbitrarily specified) water supply. Since $-K_I^{(2)}$ and $K_I^{(3)}$ quickly become much greater than $K_I^{(1)}$ as depth increases, the fracture propagation is controlled by the balance between $K_I^{(2)}$ and $K_I^{(3)}$. In turn, because $K_I^{(3)}$ increases with water level in the fracture, the fracture propagation rate is effectively limited by the filling rate.

To impose the limit on water supply we consider water leaking from a channel into an initially air-filled fracture as analogous to water leaking out of a crack in a pipe. This can be estimated by Toricelli's equation, which is commonly used in fluid dynamics to describe water leakage through small apertures [29, 60, 61]. For a crack of area A in a fluid-filled pipe under hydraulic head h, the rate of fluid loss (q) is:

$$q = CA\sqrt{2gh} \tag{6}$$

The constant C lies between 0 and 1, and depends on the fluid viscosity and crack geometry. For a low viscosity fluid such as water, leaking into a transverse linear fracture, $C \approx 0.6$ [60].

Suppose a fracture of width w_f intersects a supraglacial channel (Figs. 2 and ED4). The fracture width is assumed to be constant with time and depth, except immediately below the channel where the width can increase to w_{fc} due to viscous heat dissipation as discussed below. We assume the fracture is oriented perpendicular to the channel, has a semi-circular cross section with radius r_c, and is full of water. Water depth h in the channel varies around the perimeter from 0 at the top surface to r_c at the bottom. In polar co-ordinates (r, ϕ) with the water surface at $\phi = 0$ and channel perimeter at $r = r_c$, the total leak is the sum of many small leaks (δq) along the perimeter (Fig. ED4), i.e.,

$$\delta q = C\delta A\sqrt{2gh} \tag{7}$$

Integrating around the curved part of the perimeter (from $\phi = 0$ to $\phi = \pi$), using water depth $h = r_c \sin\phi$ and area $\delta A = w_{fc} r_c \delta\phi$, we have:

$$q = Cw_{fc}r_c^{3/2}\sqrt{2g}\int_0^{\pi}\sqrt{\sin\phi}\cdot d\phi \tag{8}$$

The integral in Eq. 8 is evaluated numerically and has a value of 2.4.

Narrow fractures formed during the spring event in west Greenland can extend hundreds of metres [13]. Therefore we consider the range $50 \leq L_f \leq 500$ m. The additional contribution of smaller streams intersecting long fractures is discussed as one of the limitations in the main text.

We next consider refreezing, since englacial ice in ice sheets is often well below the melting point (see temperature profiles in Fig. 1). We use the Alley et al. [26] estimate for the ice accretion thickness w_i, which follows Rubin [62]:

$$w_i(t) = \frac{2c(T_m - T_0)}{\sqrt{\pi}L}\sqrt{kt} \tag{9}$$

where c and Γ and k are the specific heat capacity, latent heat of fusion and thermal diffusivity of ice; T_m is the melting temperature; and T_0 is the englacial ice temperature. Noting that ice freezes on to both sides of the fracture, the remaining open fracture width after time t is $w_f - 2w_i(t)$. Refreezing was considered briefly by van der Veen [58] using this equation, but neglected as being too slow to affect the propagation of 'crevasses' (which are typically of order 1 m in width), unless hydrofracture to the bed takes 'several days or so'. More recent studies have also neglected refreezing [27, 42], but they also considered wide fractures (widths 0.1 to 5 m) which are a factor of 10 to 500 times wider than the observed cm-scale fractures we consider here.

Fracture width

In the model presented above we have imposed a simple fracture geometry in which the width w_f is constant with depth, except immediately beneath the channel. w_f is estimated using our observations of fractures at the surface. While the assumption of parallel-sided fractures has been shown to be reasonable for water-filled fractures [38], it may not hold for partially water-filled fractures. As an alternative we could have used the theoretical approach of Krawczynski et al. [38] (following Weertman [24]) to calculate how fracture width varies with depth. Taking Eqs. 3 and 4 from the supplement in Krawczynski et al. [38], we have in our notation:

$$\begin{aligned} w_f(z) = {} & M\left(\pi\sigma + \rho_i g z\right) Z_d - M\rho_w g Z_a Z_d \\ & + \frac{1}{2}M\rho_i g z^2 \ln\left(\frac{z_d + Z_d}{z_d - Z_d}\right) + \frac{1}{2}M\rho_w g(z^2 - z_a^2)\ln\left|\frac{Z_a + Z_d}{Z_a - Z_d}\right| \\ & - M\rho_w g z_a z \ln\left|\frac{z_a Z_d + zZ_a}{z_a Z_d - zZ_a}\right| + M\rho_w g z_a^2 \ln\left|\frac{Z_d + Z_a}{Z_d - Z_a}\right| \end{aligned} \tag{10}$$

where $Z_d = \sqrt{z_d^2 - z^2}$, $Z_a = \sqrt{z_d^2 - z_a^2}$, $M = 4(1-\nu)/(\pi\mu)$, μ and ν are the elastic shear modulus and Poisson's ratio for ice, and σ is the far-field tensile stress (σ_t) modified by additional terms accounting for the fracture geometry:

$$\sigma = \sigma_x' - \frac{2}{\pi}\rho_i g z_d - \rho_w g z_a + \frac{2}{\pi}\rho_w g z_a \arcsin\left(\frac{z_a}{z_d}\right) + \frac{2}{\pi}\rho_w g Z_a \tag{11}$$

Although this theory has been successfully applied to supraglacial lake drainage [38], some problems arise when water supply is limited. First, unless the fracture remains almost completely water filled, a constriction develops in the upper fracture (see Fig. ED7a). When using the stress intensity approach to calculate propagation depth, the water level is too low to prevent this constriction, which then blocks additional water flow into the fracture. If instead we impose the condition that the fracture remains completely water filled, and just use Eq. 10 to calculate the width at the surface (which is then a good estimate for the width at depth), we find the fracture steadily widens as its depth increases, soon becoming far wider than the observed cm-scale surface fractures considered here (see Fig. ED7b). Although we could conclude from this theory that deep propagation of thin fractures is not possible in cold ice – bearing in mind there is still no direct evidence of this process – it would contradict compelling indirect evidence, i.e., our observations of stream capture and moulin development by thin fractures, through several hundred metres of ice (Figs. ED1 - ED3). To enable moulin development without lake drainage, these thin fractures must under some conditions be able to propagate sufficiently deeply to connect with the subglacial drainage system.

The discrepancies between theoretical predictions and our observations should be explored further in future studies. For now we adopt the simple assumption that the fractures we observe are parallel-sided with a width that is constant in time. The one exception we consider is widening of the very top of the fracture by viscous heat dissipation, which we estimate next.

Viscous heat dissipation and drag

Viscous heat dissipation released as the water loses height in the fracture will cause some melting of the ice walls, and will exert drag that limits the water velocity.

In the water filled part of the fracture, we assume a steady vertical water velocity and assume that loss in gravitational potential energy is dissipated locally. From conservation of energy, the total wall melt at depth z for a fracture that has penetrated to depth z_d (with $z_d > z > z_a$) is:

$$w_m = \frac{\rho_w g w_f}{\Gamma \rho_i}(z_d - z) \tag{12}$$

where Γ is the latent heat of fusion of ice. Eq. 12 predicts less than 1 mm of melt for a fracture 2 cm wide penetrating the full depth of ice 1000 m thick, so it is unlikely to make an important contribution *if the melt is distributed evenly*. The case of preferential flow paths developing in partially ice-choked fractures is not considered here. Of course, viscous heat dissipation does eventually need to become important if a moulin shaft is to develop (as illustrated in the cases shown in Extended Data Figs. ED1 and ED2). In the air-filled upper part of the fracture, the aperture in the channel floor should widen quicker than the wall melting rate estimated in Eq. 12, because water flow is concentrated in the region directly under the channel rather than across the full fracture length. This process is difficult to capture in a simple model, but if we assume viscous heat dissipation is spread evenly across a length of fracture equivalent to the width of the channel ($2r_c$), the change in fracture width (w_{fc}) just beneath the channel is estimated as:

$$\frac{dw_{fc}}{dt} = \frac{q\rho_w g}{2r_c\Gamma\rho_i} \tag{13}$$

However, Eq. 13 likely overestimates melting because (1) the water should spread laterally in a thin fracture, such that $2r_c$ is a minimum estimate; and (2) as w_{fc} increases, the fracture walls exert decreasing resistance to water flow, so that the lost potential energy is increasingly used to accelerate the water locally, before eventually being dissipated at a greater depth. For now, we consider two end members: the 'slow' model which excludes any moulin growth below the channel (i.e., $dw_{fc}/dt = 0$), and the 'fast' model which includes the (likely overestimated) moulin growth in Eq. 13. In future, more elaborate models should certainly consider the processes of water flow and viscous heat dissipation in more detail, using computational fluid dynamics rather than our simple empirical approach.

As well as water supply rate, fracture propagation rate could be limited by the vertical water velocity in the fracture iself. Indeed, this limits propagation rate in the Alley et al. [26] model. In a vertical, parallel-sided fracture, the water flow rate Q (equivalent to the vertical water velocity in m s^{-1}) in their model is:

$$Q = \frac{Gw_f^3}{12\eta} \tag{14}$$

where $\eta = 1.8 \times 10^{-3}$ Pa s is the water viscosity and G is the hydraulic potential gradient. For steady vertical flow in the fracture, away from the crack tip, we can use the approximation $G = \rho_w g$. This would give $Q = 0.5$ to 4 m s^{-1} in a fracture of width 1 to 2 cm. Therefore, given that full-depth fracture propagation takes over an hour even in thin ice (propagation rate $<< 0.1$ m s^{-1}: Fig. 3), our results suggest it is the water supply to the crack rather than viscous drag within the crack that limits propagation rate of fractures beneath supraglacial streams. We reach this different conclusion to Alley et al. [26] partly because of our imposed limit on water supply, and partly because we specify fracture width w_f directly (based on our observations) rather than following their approach of calculating w_f using the elastic properties of ice, which initially yields much thinner fractures that are more prone to occlusion (see Eqs 1 to 4 in Alley et al. [26]).

Numerical solution

Now we can estimate the propagation and refreezing rates of a hydrofracture driven by supraglacial channel leakage. For propagation, van der Veen [58] used the approximation

$$\frac{dz_d}{dt} = \left(\frac{\rho_w}{\rho_i}\right)^{2/3} Q \tag{15}$$

where Q is the filling rate (in m/hr), here equivalent to $q/(L_f w_f)$. Although this yields an excellent approximation for z_d, we use the full solution (Eqs. 1 - 3) because we also want to track the upper water level when estimating ice accretion.

We assume that fractures are initially air-filled ($z_a = z_d$), and have already propagated to the maximum depth given by the condition $K_I > K_{Ic}$. This depth, d_0, is evaluated numerically using Eqs. 1 and 2. We note that both R_{xx} and K_{Ic} are poorly constrained. We have considered the respective ranges 50 to 500 kPa and 0.1 to 0.4 MPa m$^{1/2}$, but find very little sensitivity to these choices. All reported results used 100 kPa and 0.2 MPa m$^{1/2}$.

The fracture tip and water level are at $z_d(t)$ and $z_a(t)$, respectively (Fig. 2). Starting with an empty fracture ($z_d(0) = z_a(0) = d_0$), we add water to the fracture at rate q. The change in water level is:

$$\frac{dz_a}{dt} = \frac{dz_d}{dt} - \frac{q}{L_f w_f} \tag{16}$$

Eq. 16 is integrated numerically; at each time step, the new fracture depth z_d is first evaluated using the stress intensities and current water level (Eqs. 1 - 3), before calculating the new water level. In the 'slow' model q is held constant, and in the 'fast' model q increases as w_{fc} increases according to Eq. 13.

Similarly to Alley et al. [26] we do not couple water flow and ice accretion. Therefore, the ice accretion is calculated separately, using the cumulative time for which each level z has been between z_d and z_a. We then evaluate likely propagation depth by comparing the accreted ice thickness with typical fracture widths, as indicated by the stippling and hatching in Figs. 3 and 4.

Interestingly the fracture propagation rate is independent of fracture width w_f in both models. In the 'slow' model, water supply rate q is proportional to $w_f c$ (from Eq. 8), but we maintain $w_f = w_{fc}$, cancelling w_f in the denominator of Eq. 16. In the fast model where we also consider widening of the top of the fracture by viscous heat dissipation, the change in fracture width just below the channel (w_{fc}) is given by Eq. 13. Taking $w_{fc} = w_f$ at t=0, Eq. 13 is solved to give

$$w_{fc}(t) = w_f e^{\alpha t} \tag{17}$$

where α contains other constants and parameters from Eqs. 8 and 13. Hence, by substituting w_{fc} for w_f in the expression for q (Eq. 8), we again find that w_f cancels from Eq. 16. However, while the propagation rate is independent of w_f, the time taken to occlude the fracture by freezing (and hence, the likely propagation depth), and the strength of englacial warming (below), are both sensitive to this parameter.

Englacial warming

One potentially important consequence of hydrofractures, besides moulin development, is their potential to cause englacial warming. This is relevant whether or not the fracture reaches the bed, provided the water refreezes locally before draining out. Here we use a straightforward energy balance calculation to estimate warming under a range of relevant conditions (fracture densities and ice flow velocities). We consider the along-flow fracture density D_f (units: number per km per year), which is the number of fractures forming each year per unit length along a surface flow line. We have few constraints on D_f, except at moulin L41 where we have observed $D_f \geq 13$ km^{-1} yr^{-1} (surface velocity $\sim$0.15 km yr^{-1}; at least 2 new sets of fractures each year; so locally $D_f \geq 2/0.15 = 13$ km^{-1} yr^{-1}). If all the water filling the new fractures refreezes, then the equivalent volume-averaged englacial heat source Q_f (in J m^{-3} yr^{-1}) is:

$$Q_f = D_f w_f \rho_w \Gamma \tag{18}$$

The rate of englacial warming (in K yr^{-1}) due to the fractures is then

$$\frac{dT_f}{dt} = \frac{Q_f}{\rho_i c_p} = D_f w_f \frac{\rho_w}{\rho_i} \frac{\Gamma}{c_p} \tag{19}$$

This warming applies at all levels above the lower limit of fracture propagation. Although these rates appear small (Fig. 5a), their effectiveness is more apparent if considering typical flow velocities, and the many decades taken to advect ice through the ablation zone. For ice velocity V, the rate of englacial warming *per unit distance along the flow direction*, i.e. in the Lagrangian sense, is:

$$\frac{dT_f}{dx} = \frac{1}{V} \frac{dT_f}{dt} \tag{20}$$

Given that the ablation zone is tens of km across in west Greenland, warming of several K appears reasonable even with quite a low density of new fractures (Fig. 5b). For example, with V in the range 100 to 200 m yr^{-1}, warming of 1 K per 10 km could be achieved with a fracture density of 3 to 6 km^{-1} yr^{-1}.

Diurnal variability

When calculating leakage rate (Eqs 8) we have assumed that the supraglacial channel remains full. This is a reasonable assumption considering that audible fracturing is more prevalent during the evening [13], associated with hydrologically-driven ice acceleration [13, 63]. However, because hydrofractures can take >12 hours to attain the bed (Fig. 3), the effects of reduced channel water levels should be considered. Clearly this is very dependent on specific catchment size and hypsometry, snow remnants, etc., but an estimate provides some interesting insight. Suppose the water depth at the channel centre varies from a maximum r_c (late afternoon) to a minimum $0.5r_c$ (morning). For this half-filled channel the water level extends across the channel from $\phi = \pi/6$ to $\phi = 5\pi/6$. Hence, for minimum leakage the integral in Eq. 8 would be $\int_{\pi/6}^{5\pi/6} \sqrt{\sin\phi - 0.5}d\phi = 1.15$ instead of $\int_0^{\pi} \sqrt{\sin\phi}d\phi = 2.40$. If this represents the range of a sinusoidal variation in leakage, we can run the model with Eq. 8 replaced by

$$q = Cw_f r_c^{3/2} \left[1.78 + 0.63\cos(2\pi t)\right] \tag{21}$$

where time t has units of days. In this case the reduced leakage delays propagation sufficiently to make a noticeable increase in ice accretion (Figs. ED5- ED6). Characterising the temporal variability in stream flow should be worthwhile if applying this model to specific sites.

Acknowledgments. DC acknowledges support for fieldwork from UK NERC grant NE/H023879/1. AH gratefully acknowledges a research professorship from the Research Council of Norway through its Centre of Excellence funding scheme (SFF Grant 223259), Arctic Interactions funding from the University of Oulu and the Academy of Finland (PROFI4: Grant 318930) and an Arctic Five Professorship. Field observations were kindly supported by The Royal Geographical Society (Walters Kundert Fellowship), the Greenland Analogue Project (GAP-SPB), Lars Ostenfeld / Caspar Haarløv ("Into the Ice") and James Reed / Ted Giffords (BBC "Frozen Planet II").

Author contributions

DC developed the model; both authors contributed to writing the manuscript.

Competing interests

The authors declare no competing interests.

Availability of data and materials

MAR v3.11.2 data were downloaded from ftp://ftp.climato.be/fettweis/.MARv3.11.2/ (last access: 24 June 2022).

Code availability

Python scripts for the fracture propagation model are available on request from the corresponding author.

Extended data

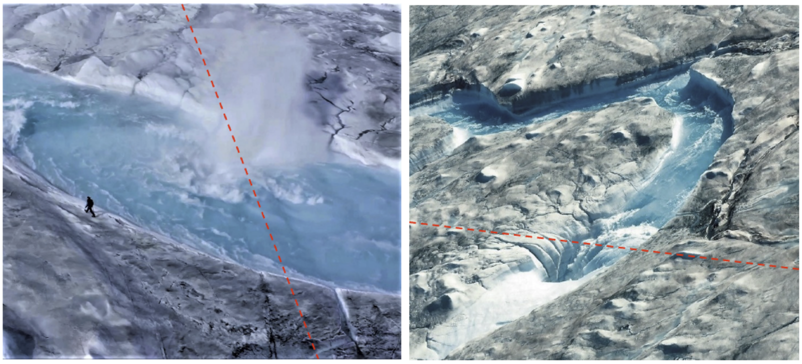

Fig. ED1 Active hydrofracture and moulin genesis where surface fractures intersected a supraglacial river on the K-Transect, West Greenland (67.124°N 49.298°W, ice thickness ∼1265 m [64, 65]). The site is close to Isunguata Sermia (labeled IS S5 in Fig. 1). Left: photo taken on 18 July 2019 when the fracture was observed to open with the onset of moulin formation and active stream interception. Right: photo taken on 25 July 2019, when the moulin had fully developed, and captured all supraglacial river discharge in an act of rapid glaciofluvial piracy. Red dashes show the approximate orientation of the surface fractures. Although this specific case is for a channel larger than the maximum considered in our model experiments, it nevertheless demonstrates that full depth hydrofracture is possible from supraglacial stream interception even through thick (>1200 m) ice - consistent with a tendency towards increasing likelihood as channel radius r_c increases in Fig. 4. The rate of development also demonstrates that enlargement of the fracture below the stream by viscous heat dissipation - as considered in our 'fast' model - is a potent process that rapidly accelerates stream capture.

Fig. ED2 Fracture zone and moulin development at Leverett Catchment site L41 (ice thickness ∼800 to 900 m). The site is close to Isunguata Sermia (labeled IS S5 in Fig. 1). Here a period of audible fracturing commenced on 3 June 2012, associated with seasonal ice flow acceleration as described by Chandler et al. [13]. Left: The fracture zone developed on 3 June and extended over 1 km across-flow. Photo taken 23 June 2012; drill is ∼1 m tall. Right: Moulin L41A, which developed on the same fracture zone. Photo taken 13 June 2012, approximately 10 days after fracturing. Diurnal variations in stream discharge were typically 3 to 8 $m^3\ s^{-1}$. [13]

Fig. ED3 Close to the margin in the Leverett catchment (ice thickness ∼400 m), where stream capture lead to the development of moulin L7 used for tracing experiments in 2011 [12]. The photo was taken 8 June 2011, 1 day after the fracture opened. The hose width is approximately 25 mm.

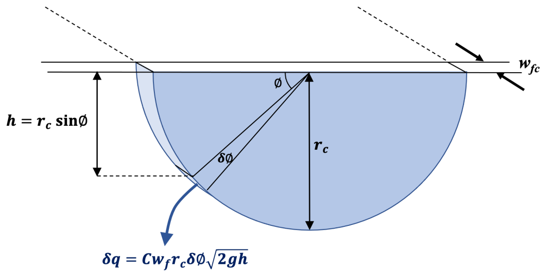

Fig. ED4 Schematic showing how water leakage is calculated in Eqs. 6 to 8. The total leak q from the channel into the fracture is treated as the sum of many small leaks δq (Eq. 7). Each small leak is calculated using Toricelli's equation (Eq. 6); these are integrated around the curved perimeter of the channel cross section from $\phi = 0$ to $\phi = \pi$ (Eq. 8). In the 'slow' model, the fracture width w_{fc} just below the channel is fixed at a constant $w_{fc} = w_f$ (as shown in Fig. 2). In the 'fast' model, w_{fc} increases with time close to the channel because turbulent heat transfer melts the ice where water is entering the fracture (see Eq. 13), but remains fixed at w_f elsewhere. Additional symbols are the parameter C in Toricelli's equation, water depth $h(\phi)$, and channel radius r_c.

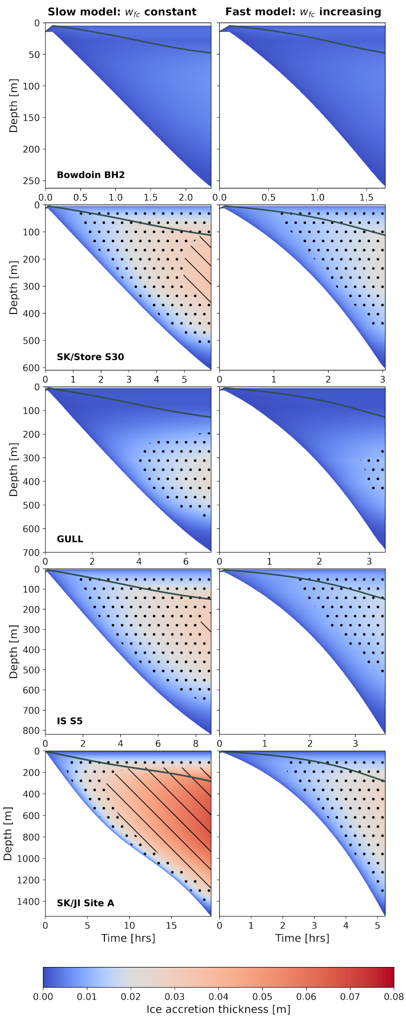

Fig. ED5 Temporal evolution of fracture propagation and ice accretion. This is the same as Fig. 3, except that diurnal changes in channel water level are included. The lower edge of the shading shows the fracture depth, and the water level is shown by the grey solid line. Shading indicates the thickness of ice accretion on to the fracture walls (Eq. 9), with stippling and hatching indicating where total ice accretion is sufficient to close fractures of width 1 or 3 cm, respectively, before they reach the bed. These examples used $L_f = 250$ m, $r_c = 1.0$ m based on observations in SW Greenland [13], and the measured borehole temperature profiles shown in Fig. 1. Note that propagation rate is independent of fracture width w_f (see Methods). The main changes from Fig. 3 are the longer propagation times, which allow thicker ice accretion and a more restricted range of conditions for full-depth hydrofracture.

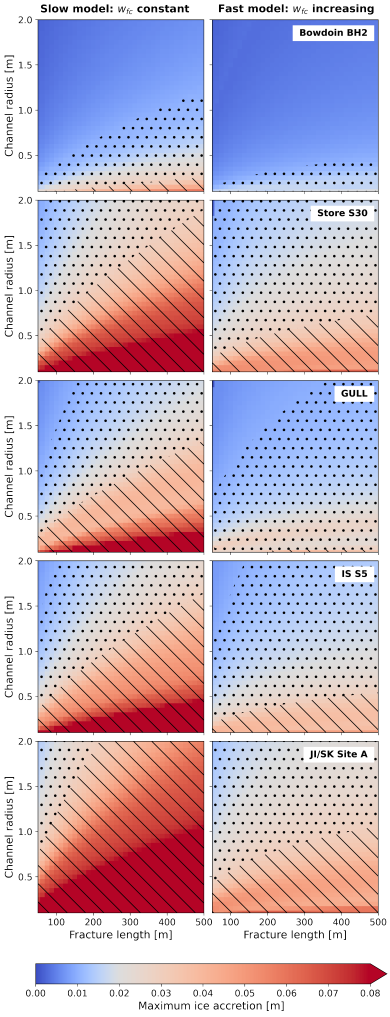

Fig. ED6 Maximum ice accretion thickness in fractures propagating to the bed. This is the same as Fig. 4, except that diurnal changes in channel water level are included. Maximum ice accretion is an indication of the minimum fracture width needed to enable full-depth hydrofracture propagation; thinner fractures will terminate before reaching the bed. Shading indicates the thickness of ice accretion (Eq. 9), with stippling and hatching indicating where total ice accretion is sufficient to close fractures of width of 1 or 3 cm, respectively. These examples used the measured borehole temperature profiles shown in Fig. 1.

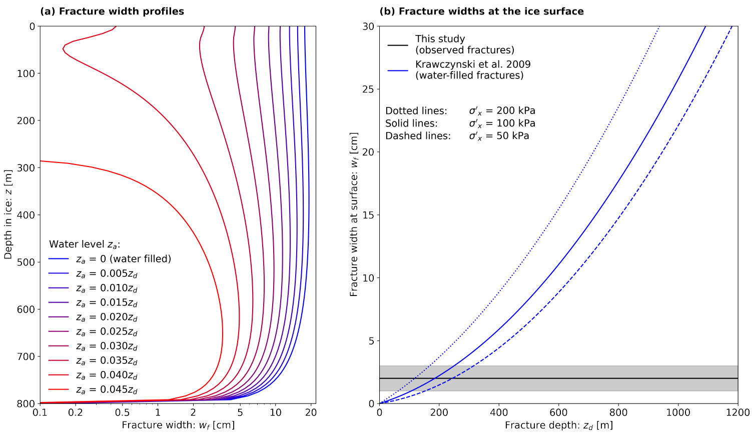

Fig. ED7 Theoretical estimates of fracture widths. (a) Fracture width profiles calculated following Krawczynski et al. [38] (Eq. 10) for partially-filled fractures that have propagated to $z_d = 800$ m. This shows how predicted fracture widths are very sensitive to water level z_a; it also shows the development of the constriction in the upper part of the fracture, once water level starts to drop below the surface (z_a/z_d decreasing just below 1), which prevents us applying their model to partially-filled fractures in our study. Qualitatively similar profiles are found for other reasonable values of z_d and σ'_x. (b) Estimates of fracture widths at the surface, for completely water-filled fractures, again following Krawczynski et al. [38] (Eq. 10; blue lines). For comparison, the black line represents the observed $\sim$2 cm-wide fractures considered in this study (grey shaded range 1 to 3 cm). Calculations used plausible tensile far-field deviatoric stresses of 50, 100 and 200 kPa (dashes, solid, dotted lines, respectively). Although such wide surface fractures are observed following lake drainage events [1, 2] they are well beyond the range of widths that we have observed to be associated with supraglacial stream capture.

References

[1] Das, S.B., Joughin, I., Behn, M.D., Howat, I.M., King, M.A., Lizarralde, D., Bhatia, M.P.: Fracture Propagation to the Base of the Greenland Ice Sheet During Supraglacial Lake Drainage. Science **320**(5877), 778–781 (2008). https://doi.org/10.1126/science.1153360

[2] Doyle, S.H., Hubbard, A.L., Dow, C.F., Jones, G.A., Fitzpatrick, A., Gusmeroli, A., Kulessa, B., Lindback, K., Pettersson, R., Box, J.E.: Ice tectonic deformation during the rapid in situ drainage of a supraglacial lake on the Greenland Ice Sheet. Cryosphere **7**(1), 129–140 (2013). https://doi.org/10.5194/tc-7-129-2013

[3] Tedesco, M., Willis, I.C., Hoffman, M.J., Banwell, A.F., Alexander, P., Arnold, N.S.: Ice dynamic response to two modes of surface lake drainage on the Greenland ice sheet. Environ. Res. Lett. **8**(3), 034007 (2013). https://doi.org/10.1088/1748-9326/8/3/034007

[4] Scambos, T., Fricker, H.A., Liu, C.-C., Bohlander, J., Fastook, J., Sargent, A., Massom, R., Wu, A.-M.: Ice shelf disintegration by plate bending and hydro-fracture: Satellite observations and model results of the 2008 Wilkins ice shelf break-ups. Earth Planet. Sci. Lett. **280**(1), 51–60 (2009). https://doi.org/10.1016/j.epsl.2008.12.027

[5] Arthur, J.F., Stokes, C., Jamieson, S.S.R., Carr, J.R., Leeson, A.A.: Recent understanding of Antarctic supraglacial lakes using satellite remote sensing. Prog. Phys. Geogr.: Earth Environ. **44**(6), 837–869 (2020). https://doi.org/10.1177/0309133320916114

[6] Christoffersen, P., Bougamont, M., Hubbard, A., Doyle, S.H., Grigsby, S., Pettersson, R.: Cascading lake drainage on the Greenland Ice Sheet triggered by tensile shock and fracture. Nat. Commun. **9**(1064), 1–12 (2018). https://doi.org/10.1038/s41467-018-03420-8

[7] Doyle, S.H., Hubbard, A., Fitzpatrick, A.A.W., van As, D., Mikkelsen, A.B., Pettersson, R., Hubbard, B.: Persistent flow acceleration within the interior of the Greenland ice sheet. Geophys. Res. Lett. **41**(3), 899–905 (2014). https://doi.org/10.1002/2013GL058933

[8] Flowers, G.E.: Hydrology and the future of the Greenland Ice Sheet. Nat. Commun. **9**(2729), 1–4 (2018). https://doi.org/10.1038/s41467-018-05002-0

[9] Williams, J.J., Gourmelen, N., Nienow, P.: Complex multi-decadal ice dynamical change inland of marine-terminating glaciers on the Greenland Ice Sheet. J. Glaciol. **67**(265), 833–846 (2021). https://doi.org/10.1017/jog.2021.31

[10] Leeson, A.A., Forster, E., Rice, A., Gourmelen, N., van Wessem, J.M.: Evolution of Supraglacial Lakes on the Larsen B Ice Shelf in the Decades Before it Collapsed. Geophys. Res. Lett. **47**(4), 2019–085591 (2020). https://doi.org/10.1029/2019GL085591

[11] Scambos, T.A., Bohlander, J.A., Shuman, C.A., Skvarca, P.: Glacier acceleration and thinning after ice shelf collapse in the Larsen B embayment, Antarctica. Geophys. Res. Lett. **31**(18) (2004). https://doi.org/10.1029/2004GL020670

[12] Chandler, D.M., Wadham, J.L., Lis, G.P., Cowton, T., Sole, A., Bartholomew, I., Telling, J., Nienow, P., Bagshaw, E.B., Mair, D., Vinen, S., Hubbard, A.: Evolution of the subglacial drainage system beneath the Greenland Ice Sheet revealed by tracers. Nat. Geosci. **6**(3), 195–198 (2013). https://doi.org/10.1038/ngeo1737

[13] Chandler, D.M., Wadham, J.L., Nienow, P.W., Doyle, S.H., Tedstone, A.J., Telling, J., Hawkings, J., Alcock, J.D., Linhoff, B., Hubbard, A.: Rapid development and persistence of efficient subglacial drainage under 900 m-thick ice in Greenland. Earth Planet. Sci. Lett. **566**, 116982 (2021). https://doi.org/10.1016/j.epsl.2021.116982

[14] Jones, C., Ryan, J., Holt, T., Hubbard, A.: Structural glaciology of Isunguata Sermia, West Greenland. J. Maps **14**(2), 517–527. https://doi.org/10.1080/17445647.2018.1507952

[15] Phillips, T., Rajaram, H., Steffen, K.: Cryo-hydrologic warming: A potential mechanism for rapid thermal response of ice sheets. Geophys. Res. Lett. **37**(20) (2010). https://doi.org/10.1029/2010GL044397

[16] Phillips, T., Rajaram, H., Colgan, W., Steffen, K., Abdalati, W.: Evaluation of cryo-hydrologic warming as an explanation for increased ice velocities in the wet snow zone, Sermeq Avannarleq, West Greenland. J. Geophys. Res. Earth Surf. **118**(3), 1241–1256 (2013). https://doi.org/10.1002/jgrf.20079

[17] Lüthi, M.P., Ryser, C., Andrews, L.C., Catania, G.A., Funk, M., Hawley, R.L., Hoffman, M.J., Neumann, T.A.: Heat sources within the Greenland Ice Sheet: dissipation, temperate paleo-firn and cryo-hydrologic warming. Cryosphere **9**(1), 245–253 (2015). https://doi.org/10.5194/tc-9-245-2015

[18] Seguinot, J., Funk, M., Bauder, A., Wyder, T., Senn, C., Sugiyama, S.: Englacial Warming Indicates Deep Crevassing in Bowdoin Glacier, Greenland. Front. Earth Sci. **8** (2020). https://doi.org/10.3389/feart.2020.00065

[19] Albrecht, T., Levermann, A.: Fracture-induced softening for large-scale

ice dynamics. Cryosphere **8**(2), 587–605 (2014). https://doi.org/10.5194/tc-8-587-2014

[20] Krug, J., Weiss, J., Gagliardini, O., Durand, G.: Combining damage and fracture mechanics to model calving. Cryosphere **8**(6), 2101–2117 (2014). https://doi.org/10.5194/tc-8-2101-2014

[21] Banwell, A.F., Caballero, M., Arnold, N.S., Glasser, N.F., Cathles, L.M., MacAyeal, D.R.: Supraglacial lakes on the Larsen B ice shelf, Antarctica, and at Paakitsoq, West Greenland: a comparative study. Ann. Glaciol. **55**(66), 1–8 (2014). https://doi.org/10.3189/2014AoG66A049

[22] Fitzpatrick, A.A.W., Hubbard, A.L., Box, J.E., Quincey, D.J., van As, D., Mikkelsen, A.P.B., Doyle, S.H., Dow, C.F., Hasholt, B., Jones, G.A.: A decade (2002–2012) of supraglacial lake volume estimates across Russell Glacier, West Greenland. Cryosphere **8**(1), 107–121 (2014). https://doi.org/10.5194/tc-8-107-2014

[23] Pope, A., Scambos, T.A., Moussavi, M., Tedesco, M., Willis, M., Shean, D., Grigsby, S.: Estimating supraglacial lake depth in West Greenland using Landsat 8 and comparison with other multispectral methods. Cryosphere **10**(1), 15–27 (2016). https://doi.org/10.5194/tc-10-15-2016

[24] Weertman, J.: Dislocation Based Fracture Mechanics. World Sci., River Edge, NJ, ??? (1996)

[25] van der Veen, C.J.: Fracture mechanics approach to penetration of surface crevasses on glaciers. Cold Reg. Sci. Technol. **27**(1), 31–47 (1998). https://doi.org/10.1016/S0165-232X(97)00022-0

[26] Alley, R.B., Dupont, T.K., Parizek, B.R., Anandakrishnan, S.: Access of surface meltwater to beds of sub-freezing glaciers: preliminary insights. Ann. Glaciol. **40**, 8–14 (2005). https://doi.org/10.3189/172756405781813483

[27] Clason, C., Mair, D.W.F., Burgess, D.O., Nienow, P.W.: Modelling the delivery of supraglacial meltwater to the ice/bed interface: application to southwest Devon Ice Cap, Nunavut, Canada. J. Glaciol. **58**(208), 361–374 (2012). https://doi.org/10.3189/2012JoG11J129

[28] Duddu, R., Bassis, J.N., Waisman, H.: A numerical investigation of surface crevasse propagation in glaciers using nonlocal continuum damage mechanics. Geophys. Res. Lett. **40**(12), 3064–3068 (2013). https://doi.org/10.1002/grl.50602

[29] Kreyzsig, E.: Advanced Engineering Mathematics 5th Edition. John Wiley and Sons, ??? (1983)

[30] Doyle, S.H., Hubbard, B., Christoffersen, P., Young, T.J., Hofstede, C., Bougamont, M., Box, J.E., Hubbard, A.: Physical Conditions of Fast Glacier Flow: 1. Measurements From Boreholes Drilled to the Bed of Store Glacier, West Greenland. J. Geophys. Res. Earth Surf. **123**(2), 324–348 (2018). https://doi.org/10.1002/2017JF004529

[31] Hubbard, B., Christoffersen, P., Doyle, S.H., Chudley, T.R., Schoonman, C.M., Law, R., Bougamont, M.: Borehole-Based Characterization of Deep Mixed-Mode Crevasses at a Greenlandic Outlet Glacier. AGU Adv. **2**(2), 2020–000291 (2021). https://doi.org/10.1029/2020AV000291

[32] Iken, A., Echelmeyer, K., Harrison, W., Funk, M.: Mechanisms of fast flow in Jakobshavns Isbræ, West Greenland: Part I. Measurements of temperature and water level in deep boreholes. J. Glaciol. **39**(131), 15–25 (1993). https://doi.org/10.3189/S0022143000015689

[33] Harrington, J.A., Humphrey, N.F., Harper, J.T.: Temperature distribution and thermal anomalies along a flowline of the Greenland ice sheet. Ann. Glaciol. **56**(70), 98–104 (2015). https://doi.org/10.3189/2015AoG70A945

[34] Colosio, P., Tedesco, M., Ranzi, R., Fettweis, X.: Surface melting over the Greenland ice sheet derived from enhanced resolution passive microwave brightness temperatures (1979–2019). Cryosphere **15**(6), 2623–2646 (2021). https://doi.org/10.5194/tc-15-2623-2021

[35] Hersbach, H., Bell, B., Berrisford, P., Hirahara, S., Horányi, A., Muñoz-Sabater, J., Nicolas, J., Peubey, C., Radu, R., Schepers, D., Simmons, A., Soci, C., Abdalla, S., Abellan, X., Balsamo, G., Bechtold, P., Biavati, G., Bidlot, J., Bonavita, M., De Chiara, G., Dahlgren, P., Dee, D., Diamantakis, M., Dragani, R., Flemming, J., Forbes, R., Fuentes, M., Geer, A., Haimberger, L., Healy, S., Hogan, R.J., Hólm, E., Janisková, M., Keeley, S., Laloyaux, P., Lopez, P., Lupu, C., Radnoti, G., de Rosnay, P., Rozum, I., Vamborg, F., Villaume, S., Thépaut, J.-N.: The ERA5 global reanalysis. Q. J. R. Meteorolog. Soc. **146**(730), 1999–2049 (2020). https://doi.org/10.1002/qj.3803

[36] Smith, L.C., Andrews, L.C., Pitcher, L.H., Overstreet, B.T., Rennermalm, Å.K., Cooper, M.G., Cooley, S.W., Ryan, J.C., Miège, C., Kershner, C., Simpson, C.E.: Supraglacial River Forcing of Subglacial Water Storage and Diurnal Ice Sheet Motion. Geophys. Res. Lett. **48**(7), 2020–091418 (2021). https://doi.org/10.1029/2020GL091418

[37] Hambrey, M.J., Murray, T., Glasser, N.F., Hubbard, A., Hubbard, B., Stuart, G., Hansen, S., Kohler, J.: Structure and changing dynamics of a polythermal valley glacier on a centennial timescale: Midre Lovénbreen, Svalbard. J. Geophys. Res. Earth Surf. **110**(F1) (2005). https://doi.org/

10.1029/2004JF000128

[38] Krawczynski, M.J., Behn, M.D., Das, S.B., Joughin, I.: Constraints on the lake volume required for hydro-fracture through ice sheets. Geophys. Res. Lett. **36**(10) (2009). https://doi.org/10.1029/2008GL036765

[39] van der Veen, C.J.: Fracture mechanics approach to penetration of bottom crevasses on glaciers. Cold Reg. Sci. Technol. **27**(3), 213–223 (1998). https://doi.org/10.1016/S0165-232X(98)00006-8

[40] McDowell, I.E., Humphrey, N.F., Harper, J.T., Meierbachtol, T.W.: The cooling signature of basal crevasses in a hard-bedded region of the Greenland Ice Sheet. Cryosphere **15**(2), 897–907 (2021). https://doi.org/10.5194/tc-15-897-2021

[41] Bartholomew, I., Nienow, P., Mair, D., Hubbard, A., King, M.A., Sole, A.: Seasonal evolution of subglacial drainage and acceleration in a Greenland outlet glacier. Nat. Geosci. **3**, 408–411 (2010). https://doi.org/10.1038/ngeo863

[42] Everett, A., Murray, T., Selmes, N., Rutt, I.C., Luckman, A., James, T.D., Clason, C., O'Leary, M., Karunarathna, H., Moloney, V., Reeve, D.E.: Annual down-glacier drainage of lakes and water-filled crevasses at Helheim Glacier, southeast Greenland. J. Geophys. Res. Earth Surf. **121**(10), 1819–1833 (2016). https://doi.org/10.1002/2016JF003831

[43] Walder, J.S.: Stability of Sheet Flow of Water Beneath Temperate Glaciers and Implications for Glacier Surging. J. Glaciol. **28**(99), 273–293 (1982). https://doi.org/10.3189/S0022143000011631

[44] Colgan, W., Rajaram, H., Abdalati, W., McCutchan, C., Mottram, R., Moussavi, M.S., Grigsby, S.: Glacier crevasses: Observations, models, and mass balance implications. Rev. Geophys. **54**(1), 119–161 (2016). https://doi.org/10.1002/2015RG000504

[45] Poinar, K., Joughin, I., Lenaerts, J.T.M., Van Den Broeke, M.R.: Englacial latent-heat transfer has limited influence on seaward ice flux in western Greenland. J. Glaciol. **63**(237), 1–16 (2017). https://doi.org/10.1017/jog.2016.103

[46] Pollard, D., DeConto, R.M., Alley, R.B.: Potential Antarctic Ice Sheet retreat driven by hydrofracturing and ice cliff failure. Earth Planet. Sci. Lett. **412**, 112–121 (2015). https://doi.org/10.1016/j.epsl.2014.12.035

[47] Lai, C.-Y., Kingslake, J., Wearing, M.G., Chen, P.-H.C., Gentine, P., Li, H., Spergel, J.J., van Wessem, J.M.: Vulnerability of Antarctica's ice shelves to meltwater-driven fracture. Nature **584**, 574–578 (2020).

https://doi.org/10.1038/s41586-020-2627-8

[48] Langley, E.S., Leeson, A.A., Stokes, C.R., Jamieson, S.S.R.: Seasonal evolution of supraglacial lakes on an East Antarctic outlet glacier. Geophys. Res. Lett. **43**(16), 8563–8571 (2016). https://doi.org/10.1002/2016GL069511

[49] Kingslake, J., Ely, J.C., Das, I., Bell, R.E.: Widespread movement of meltwater onto and across Antarctic ice shelves. Nature **544**, 349–352 (2017). https://doi.org/10.1038/nature22049

[50] Corr, D., Leeson, A., McMillan, M., Zhang, C., Barnes, T.: An inventory of supraglacial lakes and channels across the West Antarctic Ice Sheet. Earth Syst. Sci. Data **14**(1), 209–228 (2022). https://doi.org/10.5194/essd-14-209-2022

[51] Bell, R.E., Chu, W., Kingslake, J., Das, I., Tedesco, M., Tinto, K.J., Zappa, C.J., Frezzotti, M., Boghosian, A., Lee, W.S.: Antarctic ice shelf potentially stabilized by export of meltwater in surface river. Nature **544**, 344–348 (2017). https://doi.org/10.1038/nature22048

[52] Sundal, A.V., Shepherd, A., Nienow, P., Hanna, E., Palmer, S., Huybrechts, P.: Evolution of supra-glacial lakes across the Greenland Ice Sheet. Remote Sens. Environ. **113**(10), 2164–2171 (2009). https://doi.org/10.1016/j.rse.2009.05.018

[53] Selmes, N., Murray, T., James, T.D.: Fast draining lakes on the Greenland Ice Sheet. Geophys. Res. Lett. **38**(15) (2011). https://doi.org/10.1029/2011GL047872

[54] Morriss, B.F., Hawley, R.L., Chipman, J.W., Andrews, L.C., Catania, G.A., Hoffman, M.J., Lüthi, M.P., Neumann, T.A.: A ten-year record of supraglacial lake evolution and rapid drainage in West Greenland using an automated processing algorithm for multispectral imagery. Cryosphere **7**(6), 1869–1877 (2013). https://doi.org/10.5194/tc-7-1869-2013

[55] Rivalta, E., Taisne, B., Bunger, A.P., Katz, R.F.: A review of mechanical models of dike propagation: Schools of thought, results and future directions. Tectonophysics **638**, 1–42 (2015). https://doi.org/10.1016/j.tecto.2014.10.003

[56] Van Der Veen, C.J., Whillans, I.M.: Force Budget: I. Theory and Numerical Methods. J. Glaciol. **35**(119), 53–60 (1989). https://doi.org/10.3189/002214389793701581

[57] Broek, D.: Elementary Engineering Fracture Mechanics, 4th Edition. Kluwer Academic Publishers, Dordrecht, ??? (1986)

[58] van der Veen, C.J.: Fracture propagation as means of rapidly transferring surface meltwater to the base of glaciers. Geophys. Res. Lett. **34**(1) (2007). https://doi.org/10.1029/2006GL028385

[59] Weertman, J.: Can a water-filled crevasse reach the bottom surface of a glacier? IASH. Publ **95** (1973)

[60] Franchini, M., Lanza, L.: Use of Torricelli's Equation for Describing Leakages in Pipes of Different Elastic Materials, Diameters and Orifice Shape and Dimensions. Procedia Eng. **89**, 290–297 (2014). https://doi.org/10.1016/j.proeng.2014.11.190

[61] De Marchis, M., Milici, B.: Leakage Estimation in Water Distribution Network: Effect of the Shape and Size Cracks. Water Resour. Manage. **33**(3), 1167–1183 (2019). https://doi.org/10.1007/s11269-018-2173-4

[62] Rubin, A.M.: Propagation of Magma-Filled Cracks. Annu. Rev. Earth Planet. Sci. **23**(1), 287–336 (1995). https://doi.org/10.1146/annurev.ea.23.050195.001443

[63] Bartholomew, I., Nienow, P., Sole, A., Mair, D., Cowton, T., King, M.A.: Short-term variability in Greenland Ice Sheet motion forced by time-varying meltwater drainage: Implications for the relationship between subglacial drainage system behavior and ice velocity. J. Geophys. Res. Earth Surf. **117**(F3) (2012). https://doi.org/10.1029/2011JF002220

[64] Lindbäck, K., Pettersson, R., Doyle, S.H., Helanow, C., Jansson, P., Kristensen, S.S., Stenseng, L., Forsberg, R., Hubbard, A.L.: High-resolution ice thickness and bed topography of a land-terminating section of the Greenland Ice Sheet. Earth Syst. Sci. Data **6**(2), 331–338 (2014). https://doi.org/10.5194/essd-6-331-2014

[65] Booth, A.D., Clark, R.A., Kulessa, B., Murray, T., Carter, J., Hubbard, A.: Thin-layer effects in glaciological seismic amplitude-versus-angle (AVA) analysis: implications for characterising a subglacial till unit, Russell Glacier, West Greenland. Cryosphere **6**(4), 909–922 (2012). https://doi.org/10.5194/tc-6-909-2012